DOI 10.59887/2073–6673.2023.16(2)-5

УДК 551.466.7

© *B. A. Kagan**, *A. A. Timofeev*, 2023
© Translation from Russian: *E. S. Kochetkova*, 2023
Shirshov Institute of Oceanology, Russian Academy of Sciences, 36 Nakhimovsky Prosp., Moscow, 117997, Russia
*kagan.ba@spb.ocean.ru

HIGH-RESOLVING MODELING OF THE SURFACE SEMIDIURNAL M_2 TIDE IN THE EAST-SIBERIAN SEA

Received 13.12.2022, Revised 21.04.2023, Accepted 02.05.2023

Abstract

In the framework of a high-resolving version of the 3D finite-element hydrostatic model QUODDY-4 we have simulated the fields of dynamic characteristics (amplitudes and phases of tidal elevations and barotropic tidal velocity ellipses) corresponding to the surface semidiurnal M_2 tide in the no-ice East-Siberian Sea. It is shown that the obtained tidal chart has a complex structure, determined by 4 real amphidromes of left rotation which are induced by interference of counter-coming progressive Poincare waves in the southern part of the sea, 1 fake amphidrome with the center upon the Novaya Sibir Isl. and 4 small-scale amphidromes caused by interference of counter-coming Kelvin waves, from which 3 are formed in the narrow straits in the region of Bolshoy and Maly Lyahovsky Isls. and 1 near the entrance of the Chaunskaya Guba. Tidal amplitudes in the vicinity of the Novaya Sibir Isl. achieve 20–30 cm, whereas in the remaining part of the sea they are comparatively small and do not exceed 5–10 cm. Accordingly, the field of barotropic tidal velocities in the north-western part of the sea basically consists of high values (they are tens of cm/s), but in the other parts of the sea barotropic velocities are small (lower then 10 cm/s) and their field has a band structure. The fields of the averaged (over a tidal cycle) integrated in depth constituents of the barotropic tidal energy budget (namely, the barotropic tidal energy density, the advective transport and the horizontal wave flux per unit length of this energy and the rate of its dissipation due to the bottom friction) are presented. Also, a comparison of predicted tidal elevations with the mareographic level measurement data states that an estimate of their agreement may be considered as satisfactory taking into account that the tidal amplitudes in the sea as a whole are small.

Keywords: modeling, surface semidiurnal tide, surface tidal elevations, barotropic tidal velocities, barotropic tidal energy budget, the East-Siberian Sea

© *Б. А. Каган**, *А. А. Тимофеев*, 2023
© Перевод с русского: *Е. С. Кочеткова*, 2023
Институт океанологии им. П.П. Ширшова РАН, 117997, Россия, Москва, Нахимовский проспект, 36.
*kagan.ba@spb.ocean.ru

ВЫСОКОРАЗРЕШАЮЩЕЕ МОДЕЛИРОВАНИЕ ПОВЕРХНОСТНОГО ПОЛУСУТОЧНОГО ПРИЛИВА M_2 В ВОСТОЧНО-СИБИРСКОМ МОРЕ: ЕГО ДИНАМИКА И ЭНЕРГЕТИКА

Статья поступила в редакцию 13.12.2022, после доработки 21.04.2023, принята в печать 02.05.2023

Аннотация

В рамках высокоразрешающей версии трехмерной конечно-элементной гидростатической модели QUODDY-4 воспроизведены поля динамических характеристик (амплитуды и фазы приливных колебаний уровня и эллипсов баротропной приливной скорости), отвечающих поверхностному полусуточному приливу M_2 в безлёдном Восточно-Сибирском море. Показано, что соответствующая приливная карта моря включает 4 реальные амфидромии левого вращения, обязанные своим существованием интерференции встречных прогрессивных волн Пуанкаре в южной части моря, 1 ложную амфидромию с центром на о. Новая Сибирь и 4 мелкомас-

Ссылка для цитирования: *Каган Б.А.*, *Тимофеев А.А.* Высокоразрешающее моделирование поверхностного полусуточного прилива M_2 в Восточно-Сибирском море: его динамика и энергетика // Фундаментальная и прикладная гидрофизика. 2023. Т. 16, № 2. С. 64–72. doi:10.59887/2073–6673.2023.16(2)-5
For citation: *Kagan B.A.*, *Timofeev A.A.* High-Resolving Modeling of the Surface Semidiurnal M_2 Tide in the East-Siberian Sea. *Fundamental and Applied Hydrophysics*. 2023, 16, 2, 64–72. doi:10.59887/2073–6673.2023.16(2)-5

штабные амфидромии, обусловленные интерференцией встречных волн Кельвина. Из них 3 образуются в узких проливах, расположенных в окрестности о-вов Большой и Малый Ляховский и 1 — на входе в Чаунскую губу. В свою очередь, баротропная приливная скорость в области максимума в северо-западной части моря достаточно высока (достигает нескольких десятков см/с), а за пределами максимума ее поле имеет полосчатую структуру, в которой баротропная скорость не превышает 10 см/с. Приводятся поля средних (за приливный цикл) интегральных по глубине составляющих бюджета баротропной приливной энергии (плотности энергии, ее адвективного переноса, горизонтального волнового потока и скорости диссипации за счет придонного трения). Сравнение модельных значений приливных колебаний уровня с данными его мареографных измерений приводит к заключению, что оценка их соответствия может быть признана удовлетворительной, учитывая сравнительно небольшие амплитуды прилива в море в целом.

Ключевые слова: моделирование; поверхностный полусуточный прилив; приливные колебания уровня и приливные скорости; бюджет баротропной приливной энергии; Восточно-Сибирское море

1. Introduction

Prior to the final stage of ocean tides' modeling, the authors of [1] dedicated significant efforts to address the existing knowledge gap regarding the surface semidiurnal tide M_2 in the Arctic Ocean, particularly in the East Siberian Sea. At that time, information about this tide was extremely limited. Subsequently, the research continued in [2—4], leading to the discovery that the tidal characteristics of this sea comprise between 2 and 4 amphidromes of unknown origin. Additionally, a false amphidrome centered on the Novaya Sibir and Kotelny Islands was identified. However, it is important to note that the tidal maps provided in [1—4], with the exception of the one presented in [4], were generated using low-resolution models. Consequently, they require reassessment within models that offer higher resolution. Given this consideration, our approach is as follows: first, utilizing a high-resolution version of the three-dimensional finite element hydrostatic model QUODDY-4, we obtain a new tidal map of the sea, specifically focusing on the M_2 harmonic of the surface tide. Our objective is to determine whether this new map aligns with the existing understanding of the sea. To achieve this, we determined the number and origin of the amphidromes depicted in the map and compared the model's amplitude and phase values of tidal level oscillations measured by tide gauges. The satellite altimetry data and in situ measurements of tidal current velocities were not incorporated into our analysis. The available satellite altimetry data proved to be insufficient, and surprisingly, the latter were absent completely in fact. Second, we examined the previously unexplored tidal cycle average fields of depth-integrated components of the barotropic tidal energy budget, namely, the density, advective transport, horizontal wave flux of this energy, and the dissipation rate caused by bottom friction. The primary objective of this communication was to address these two aspects.

2. QUODDY-4 model in homogeneous sea approximation

It has been routinely observed that there is minimal difference between surface tides in a stratified and a homogeneous sea. This finding has led to the practice of replacing a stratified approximation with a homogeneous when simulating surface tides. In keeping with this tradition, we employ the high-resolution version of the three-dimensional finite element hydrostatic model QUODDY-4 in a homogeneous approximation to replicate the surface semidiurnal tide M_2 in the East Siberian Sea.

The model was described in detail in [5]. To prevent repetition, we confined ourselves to listing the model equations for homogeneous sea approximation and explaining the underlying physical assumptions for certain boundary conditions. In the homogeneous sea approximation, the QUODDY-4 model included the two-dimensional generalized wave continuity equation for sea level disturbances, untransformed equations of motion in the Boussinesq approximation for horizontal velocity, evolutionary equations for turbulence characteristics such as turbulent kinetic energy (TKE) and turbulence scale, a three-dimensional continuity equation used to determine vertical velocity, a hydrostatic equation, and an approximate similarity relation for the vertical turbulent viscosity coefficient. After transferring the terms characterizing the advection effects and horizontal turbulent momentum diffusion to a previous timestep, the above model equations were solved as a system of non-stationary one-dimensional (vertically) inhomogeneous differential equations. This approach allowed for a comprehensive representation of the dynamics within the model.

The boundary conditions for the TKE at the sea's free surface and the closest to the bottom level, were set by the Dirichlet condition. This condition arose from the approximate balance between TKE production and dissipation, assuming the turbulence scale is in accord with the law of the wall, which is linking the TKE to the square of the fric-

tion velocity. Regarding the estimation of horizontal velocity at the free surface, the vertical turbulent momentum flux was set to zero, while at the nearest to the bottom computational level, it was parameterized using a quadratic drag law with a drag coefficient of 5×10^{-3}. The vertical velocity at the free surface was determined by the kinematic relation, as is customary. Vertical mixing was described using a 2.5-level turbulent closure scheme [6], while the horizontal turbulent diffusion coefficient was defined by the Smagorinsky formula [7]. The remaining boundary conditions and their parameters were assumed to be consistent with those in the original version of the model [5].

The finite element mesh employed in the model has an average horizontal resolution of 3.5 km across the sea area. In order to discretize the barotropic Rossby deformation radius of 219.9 km, 63 finite elements are utilized. Additionally, a terrain-following vertical coordinate is introduced, incorporating layers of varying thickness along the vertical axis. The sea depth is divided into 40 layers, with the layers condensing as they approach the free surface and the sea bottom. To ensure numerical stability and accuracy, a time step of 11.2 seconds is selected. This time step is determined by the method employed for solving the model equations along the vertical axis, as discussed earlier.

In this study, the tidal frequency is assumed to be equivalent to the frequency of the M_2 harmonic, which represents the tide forcing and correspond to those obtained from the high-resolution Arctic tidal model [4], which incorporates additional satellite altimetry data.

The model equations are integrated until a quasiperiodic state is reached, which is defined as the decrease of the change in the depth-integrated barotropic tidal energy density averaged over both the tidal cycle and the entire sea area, below 0.2%. It takes 23 tidal cycles from the initiation for this condition to be met.

3. Simulation results

As previously discussed, the surface semidiurnal tide M_2 in the East Siberian Sea exhibits a complex structure. The model tidal map of the M_2 harmonic in figure 1 reveals the presence of four real counterclockwise amphidromes in the southern part of the sea. Additionally, there is one false amphidromy centered on Novaya Sibir isl. and four small-scale amphidromes, with three located to the west and south of Bolshoy and Maly Lyakhovsky isl., and one situated at the entrance to Chaunskaya Guba. The formation of the four large-scale counterclockwise amphidromes can be attributed to the interference of counter-propagating progressive Poincare waves occurring in the southern region of the sea, along the mainland coast and the western coast of Wrangel Island.Three of the small-scale amphidromes are formed due to the interference of counter-propagating Kelvin waves propagating through the narrow straits near the aforementioned islands. The fourth small-scale amphidrome is formed due to the existence of a relatively narrow entrance to Chaunskaya Guba. Note a significant increase in tidal level oscillation amplitudes is observed near Novaya Sibir Island, where amplitudes reach values of 20—30 cm, in contrast to the rest of the sea with smaller tidal amplitudes, ranging from 5—10 cm.

Figure 2 illustrates the modeled field of barotropic tidal velocity ellipses. This field exhibits a distinctive pattern characterized by a velocity maximum in the northwestern part of the sea and a banded structure throughout the rest of the sea. The velocity maximum exhibits high values, reaching several tens of centimeters per second, in contrast to other parts of the sea with relatively small and almost zero velocities. The structure appears to have four bands in these areas. One band adjoins the northern open boundary of the sea, where the barotropic velocities are close to zero. Other lays southward with moderate velocity values. Further south, another band emerges where the velocities gradually decrease as distance from the north increases. Finally, near the mainland, a fourth band appears where the velocities diminish to zero. Of particular interest is the circulation pattern around Novaya Sibir Island and fragments of a similar cycle around Wrangel Island.

The root-mean-square absolute vector error for determining the amplitudes and phases of tidal level oscillations in the East Siberian Sea was estimated to be 4.1 cm based on 10 points of tide gauge measurements. This value is only 1.1 cm larger than the error in the model [4], which assimilates tidal empirical data, including satellite altimetry data. In contrast, the error in model [1], which does not incorporate data assimilation like our model, has an error of 7.5 cm. The significant difference in errors between these models may be attributed, in part, to choices of spatial resolutions.

Turning to a discussion of the fields of energy characteristics (their definitions are given in [8]), we begin with the field of the average (over a tidal cycle) depth-integrated density of the total (kinetic + potential) barotropic tidal energy, which exhibits a banded structure similar to the field of ellipses of the barotropic tidal velocities (Fig. 3). In this case there are three prominent maxima. The strongest maximum is located in the

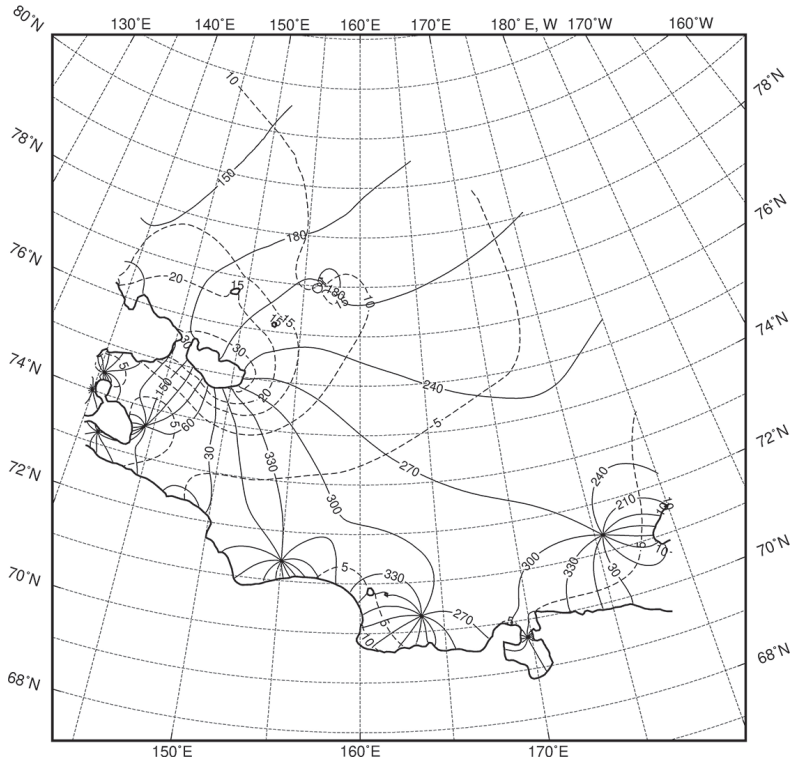

Fig. 1. Fields of isoamplitudes (dashed lines, cm) and isophases (solid lines, deg.) of tidal elevations for the M_2 harmonic in the East-Siberian Sea

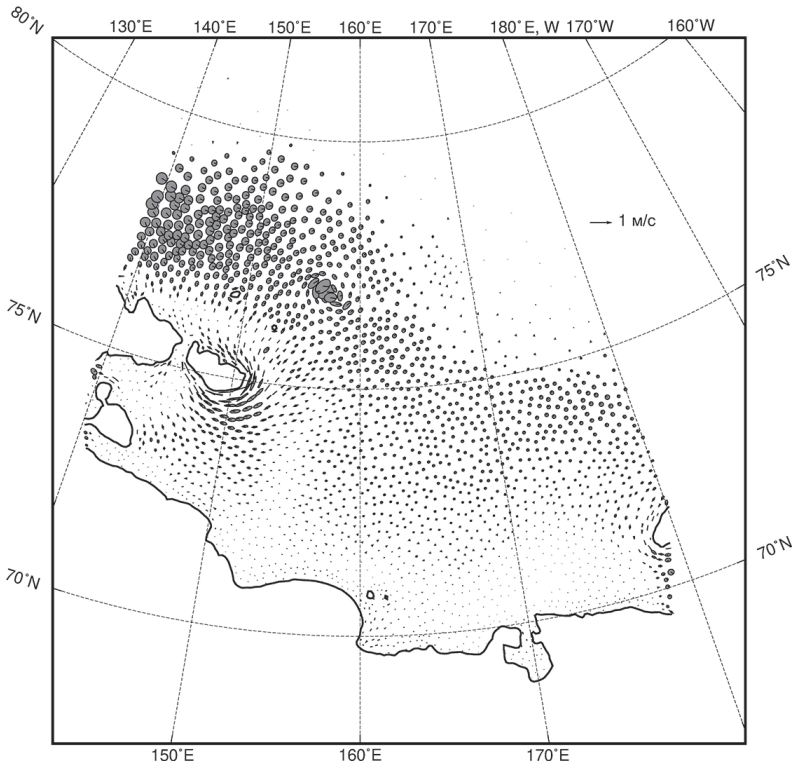

Fig. 2. Field of ellipses of the barotropic tidal velocities in the East-Siberian Sea. Ellipses with clockwise rotation of the velocity vector are shaded, with counterclockwise are not

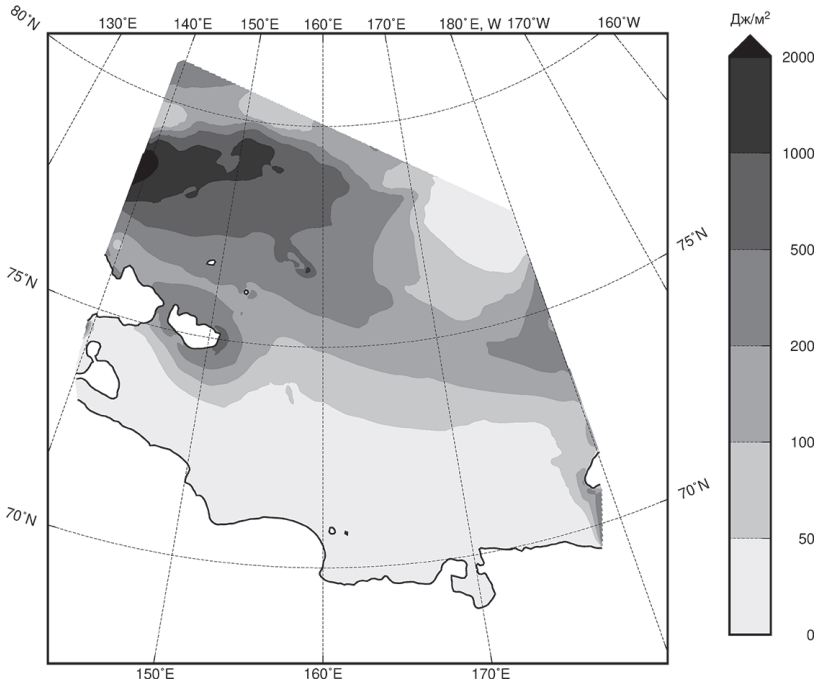

Fig. 3. Field of the averaged (over a tidal cycle) integrated in depth total (kinetic + potential) barotropic tidal energy density in the East-Siberian Sea

northwestern part of the sea, another is near Novaya Sibir isl., and the third is in the vicinity of the central part of the eastern open border of the sea. It is worth noting that the variable systematically decreases with distance from the coastline of the islands, resulting in velocity maxima around Novaya Sibir isl. and the eastern border that resemble circular shapes. Also note a significant decrease in the variable to 50 J/m^2 or less when approaching the mainland coastline. The average depth-integrated density of barotropic tidal energy over both the tidal cycle and the entire area of the sea is measured at 102.6 J/m^2.

According to Fig. 4, the average (over a tidal cycle) depth-integrated advective transport of kinetic barotropic tidal energy is presented by a combination of individual so-called gyres and multidirectional flows of this energy. These gyres are primarily observed around Novaya Sibir, Bolshoi and Maly Lyakhovsky Islands, as well as Wrangel Island. They also occur in the open sea, specifically to the north of Cape Shelagsky, along the Kolyma coast, Gusinaya Bay, and near the northwestern maximum of the variable. It is important to note that these gyres weaken as they approach the northern open boundary of the sea and the mainland coastline. Additionally, the multidirectional flows also exhibit a clear weakening.

The field depicted in Figure 5, representing the average depth-integrated horizontal wave flux of potential barotropic tidal energy, exhibits a more structured pattern compared to the advective transport field (compare Figures 4 and 5). Both fields display three maxima in the northwestern part of the sea, near Novaya Sibir Island, and in the vicinity of the eastern open border of the sea. However, there is a notable distinction: the first field demonstrates a more organized structure than the second. This contrast becomes evident upon comparing the two fields. The primary feature is the horizontal wave flux structure associated with the influx into the sea through the northern and eastern open boundaries. Subsequently, both branches of the flux extend southwestward, gradually turning westward leaving the East Siberian Sea and entering the Laptev Sea through the western open boundary. It is also important to note the significant disparity between the advective transport and the horizontal wave flux: the latter is two orders of magnitude greater than the former.

The field representing the average rate of dissipation of barotropic tidal energy due to bottom friction shows similarities to the field of barotropic tidal energy density. It exhibits three maxima and a banded structure beyond them. Two of the maxima mentioned earlier reach a dissipation rate of 10^{-2} W/m^2, while the third exceeds 10^{-3} W/m^2. A similar trend of dissipation occurs towards the east. In the open sea, the banded structure

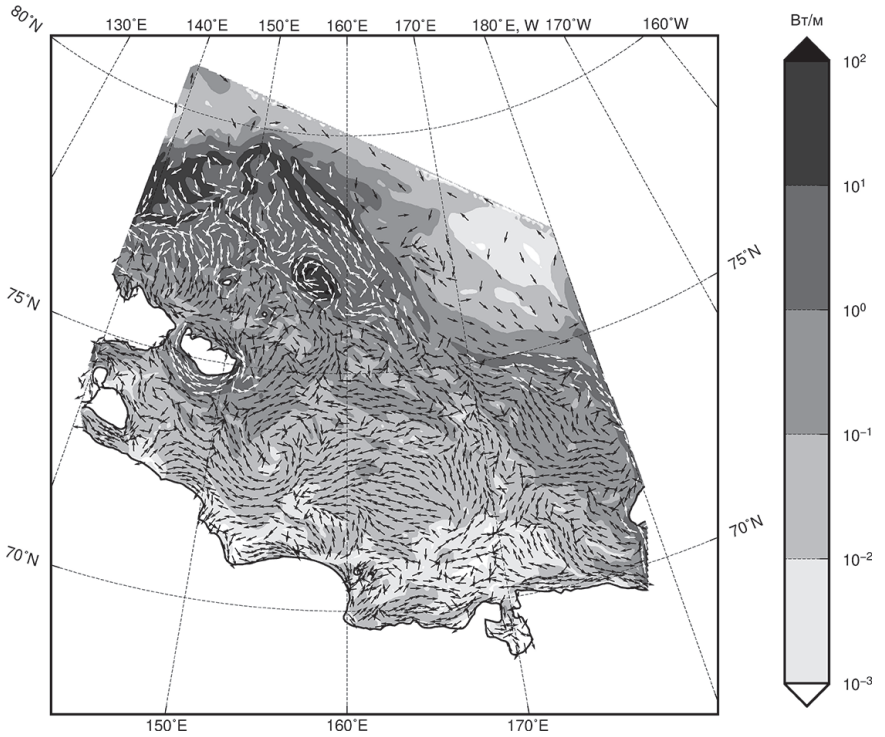

Fig. 4. Field of the averaged (over a tidal cycle) integrated in depth advective transport of kinetic barotropic tidal energy in the East-Siberian Sea. Arrows indicate the transport direction, shades of gray — transport values

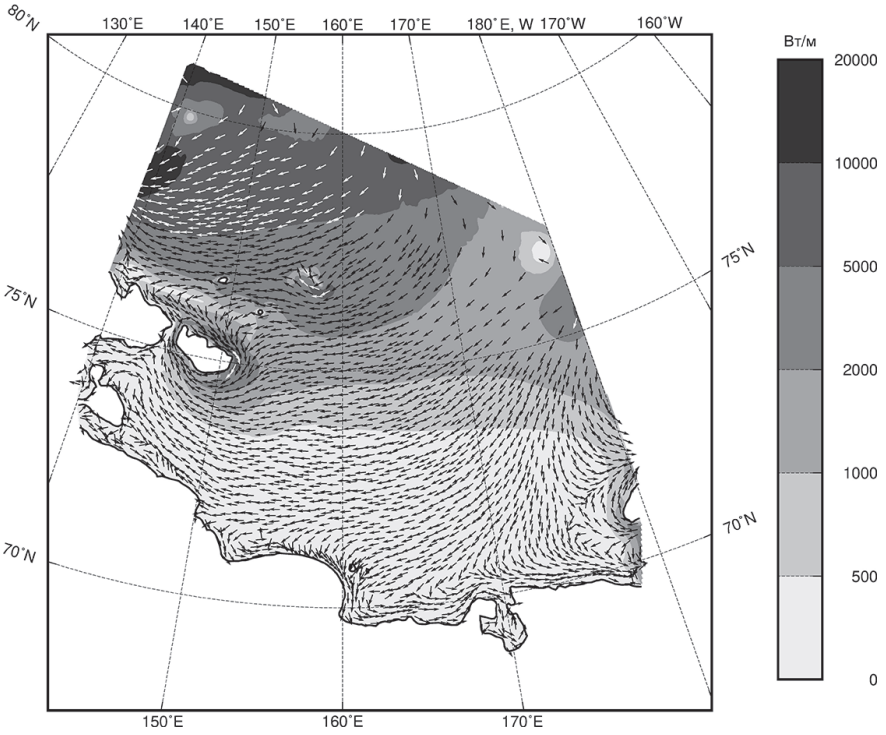

Fig. 5. Field of the averaged (over a tidal cycle) integrated in depth horizontal wave flux of potential barotropic tidal energy in the East-Siberian Sea. Explanations see in Fig. 4

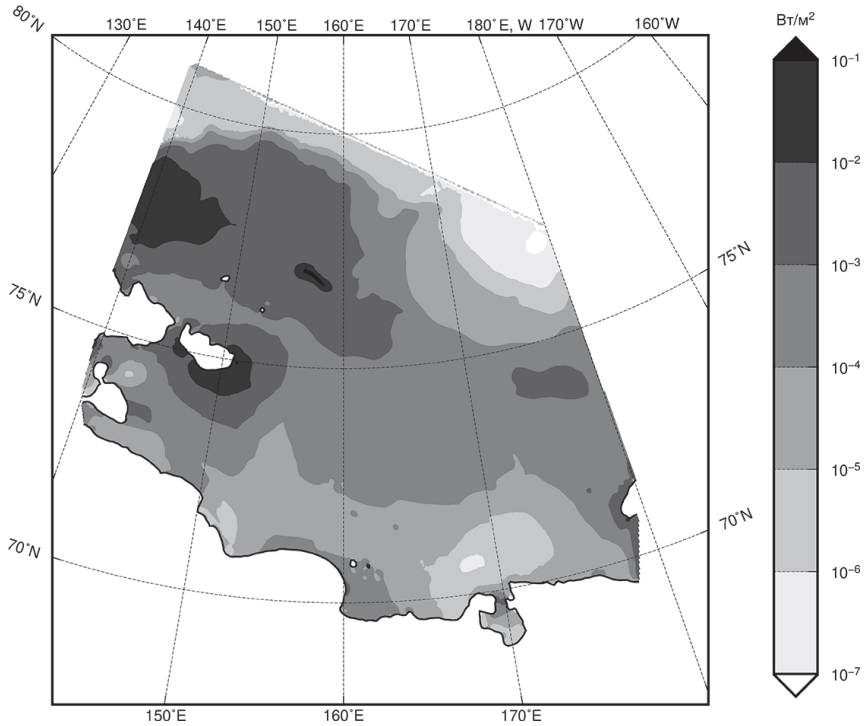

Fig. 6. Field of the averaged (over a tidal cycle) dissipation rate of barotropic tidal energy in the East-Siberian Sea

of dissipation is quite pronounced. Along the coastal areas of the mainland, the dissipation ranges from 10^{-4} to 10^{-3} W/m^2 or lower, primarily due to the weakening of barotropic tidal velocities. The average dissipation rate, considering the entire tidal cycle and the sea area, is calculated to be 1.8×10^{-3} W/m^2.

Thus, having the average values of density and dissipation rate of barotropic tidal energy available, we can estimate the dissipation time, which is the ratio of these variables. In this case, the simulated dissipation time in the East Siberian Sea is 3 hours, approximately twice as long as in the Laptev Sea [9]. This increase in dissipation time in the East Siberian Sea can be attributed to a corresponding decrease in dissipation compared to the values observed in the Laptev Sea. This decrease is primarily caused by the weakening of barotropic tidal velocities in the East Siberian Sea.

4. Conclusion

The dynamic and energy characteristics of the surface semidiurnal tide M_2 in the ice-free East Siberian Sea were simulated Using the high-resolution version of the three-dimensional finite element hydrostatic model QUODDY-4. The model reveals a complex structure in the field of isoamplitudes and isophases of tidal level fluctuations, including displays four real counterclockwise amphidromes in the southern part of the sea, resulting from the interference of opposing progressive Poincaré waves. Additionally, there is one false amphidromy centered on Novaya Sibir Island. Furthermore, four small-scale amphidromes are observed, which originate from the interference of opposing Kelvin waves propagating through narrow straits in the region of Bolshoi and Malyi Lyakhovsky Islands and through the entrance to Chaunskaya Guba. A significant increase in the amplitudes of tidal level oscillations (up to 30 cm) in the vicinity of New Siberia Island were registered as well as intensification of barotropic tidal velocities in the northwestern part of the sea and near the northern open boundary. Moreover, so-called velocity gyres of tidal currents, have been identified around Novaya Sibir and Wrangel Islands. In the eastern and central parts of the sea and especially along the coastline of the mainland, the ellipses of barotropic tidal velocities degenerate into points.

The root mean square absolute vector error in the determination of amplitudes and phases of tidal level oscillations is reported to be 4.1 cm. This value is compared with the results of two models, [1] and [4].

In Model [1], which does not incorporate assimilation of empirical tide data, the error is 7.5 cm. In Model [4], which includes observational data assimilation, the error is reduced down to 3.0 cm. Model [4] and our model show that the agreement between model estimates and observational data improves through both assimilation of observational data and a decrease in spatial resolution. The current models have a resolution of 10' and 5 km, respectively [1][4]. However, it is premature to determine which method is preferable. A larger number of comparisons is needed before drawing any conclusions.

This study presents, for the first time, the fields of average depth-integrated components of the barotropic tidal energy budget, specifically, including the barotropic tidal energy density, advective transport, horizontal wave flux of energy, and the rate of energy dissipation due to bottom friction.

Funding

This work was performed within the framework of the state assignment (theme FMWE-2021–0014).

References

1. *Kowalik Z.*, *Proshutinsky A. Yu.* The Arctic Ocean tides. In: The Polar Oceans and their role in shaping the global environment. *Geophys. Monogr. Ser.*, Vol. 85, Eds. O.M. Johanessen et al., *AGU*, *Washington*, *D.C.* 1994, P. 137–158. doi:10.1029/GM085p0137. doi:10.1029/GM085p0137
2. *Proshutinsky A. Yu.* Semidiurnal tides in the Arctic Ocean from modeling results. *Trudy AANII.* 1993, 429, 29–44 (in Russian).
3. *Polyakov I.V.*, *Dmitriev N.E.* M2 tide in the Arctic Ocean: Structure of a barotropic tide. *Meteorologiya i Gidrologiya.* 1994, 1, 56–68 (in Russian).
4. *Padman L.*, *Erofeeva S.* A barotropic reverse tidal model for the Arctic Ocean. *Geophysical Research Letters.* 2004, 31(2), L02303. doi:10.1029/2003GL019003
5. *Ip J.T.C.*, *Lynch D.R.* QUODDY-3 User's Manual: Comprehensive coastal circulation simulation using finite elements: Nonlinear prognostic time-stepping model. Report Number NML-95–1, Thayer School of Engineering, Darthmouth College, Hanover, New Hampshire, 1995, 46 p. URL: http://www-nml.dartmouth.edu/Publications/internal_reports/NML-95-1/95-1/Q3_3.ps
6. *Mellor G.L.*, *Yamada T.* Development of a turbulence closure model for geophysical fluid problems. *Reviews of Geophysics and Space Physics.* 1982, 20(4), 851–875. doi:10.1029/RG020i004p00851
7. *Smagorinsky J.* General circulation experiments with the primitive equations. *Mon. Wea. Rev.* 1963, 91(3), 99–164. doi:10.1175/1520–0493(1963)091<0099: GCEWTP>2.3.CO;2
8. *Kagan B.A.*, *Timofeev A.A.* Dynamics and energetics of surface and internal semidiurnal tides in the White Sea. *Izvestiya, Atmospheric and Oceanic Physics.* 2005, 41(4), 498–512.
9. *Kagan B.A.*, *Timofeev A.A.* Dynamics and energetics of tides in the Laptev Sea: The results of high-resolving modeling of the surface semidiurnal tide M_2. *Fundamental and Applied Hydrophysics.* 2020, 13(1), 15–23 doi:10.7868/S2073667320010025 (in Russian).

Литература

1. *Kowalik Z.*, *Proshutinsky A. Yu.* The Arctic Ocean tides // The Polar Oceans and their role in shaping the global environment. Geophys. Monogr. Ser., Vol. 85, Eds. O.M. Johanessen et al., AGU, Washington, D.C. 1994. P. 137–158. doi:10.1029/GM085p0137
2. *Прошутинский А.Ю.* Полусуточные приливы Северного Ледовитого океана по результатам моделирования // Труды ААНИИ. 1993. Вып. 429. С. 29–44.
3. *Поляков И.В.*, *Дмитриев Н.Е.* Прилив M_2 в Северном Ледовитом океане. Структура баротропного прилива // Метеорология и гидрология. 1994. № 1. С. 56–68.
4. *Padman L.*, *Erofeeva S.* A barotropic reverse tidal model for the Arctic Ocean // Geophys. Res. Lett. 2004. Vol. 31. L02303. doi:10.1029/2003GL019003
5. *Ip J.T.C.*, *Lynch D.R.* QUODDY-3 User's Manual: Comprehensive coastal circulation simulation using finite elements: Nonlinear prognostic time-stepping model. Report Number NML-95–1, Thayer School of Engineering, Darthmouth College, Hanover, New Hampshire, 1995, 46 p. URL: http://www-nml.dartmouth.edu/Publications/internal_reports/NML-95-1/95-1/Q3_3.ps
6. *Mellor G.L.*, *Yamada T.* Development of a turbulence closure model for geophysical fluid problems // Rev. Geophys. Space Phys. 1982. Vol. 20, No. 4. P. 851–875. doi:10.1029/RG020i004p00851

7. *Smagorinsky J.* General circulation experiments with the primitive equations // Mon. Wea. Rev. 1963. Vol. 91, No. 3. P. 99–164. doi:10.1175/1520–0493(1963)091<0099: GCEWTP>2.3.CO;2
8. *Каган Б.А.*, *Тимофеев А.А.* Динамика и энергетика поверхностных и внутренних полусуточных приливов в Белом море // Известия РАН. Физика атмосферы и океана. 2005. Т. 41, № 4. С. 550–566.
9. *Каган Б.А.*, *Тимофеев А.А.* Динамика и энергетика полусуточных приливов в море Лаптевых: результаты высокоразрешающего моделирования поверхностного прилива M_2 // Фундаментальная и прикладная гидрофизика. 2020. Т. 13, № 1. С. 15–23. doi:10.7868/S2073667320010025

About the authors

Kagan, Boris A., РИНЦ Author ID: 1171, ORCID ID: 0000-0003-0637-3636, Scopus Author ID: 7005584755, WoS ResearcherID: AAD-1931–2021, kagan.ba@spb.ocean.ru

Timofeev, Andrey A., РИНЦ Author ID: 69284, ORCID ID: 0009-0009-3680-3220, Scopus Author ID: 57208159130, WoS ResearcherID: AAB-4597–2021, timofeev.aa@spb.ocean.ru